THE JOURNAL OF BIOLOGICAL CHEMISTRY VOL. 289, NO. 9, pp. 5970–5985, February 28, 2014

Yeast Cells Expressing the Human Mitochondrial DNA Polymerase Reveal Correlations between Polymerase Fidelity and Human Disease Progression*[S]

Received for publication, October 10, 2013, and in revised form, January 7, 2014 Published, JBC Papers in Press, January 7, 2014, DOI 10.1074/jbc.M113.526418

Yufeng Qian[‡1], **Aashiq H. Kachroo**[‡§], **Christopher M. Yellman**[‡§], **Edward M. Marcotte**[‡§¶], **and Kenneth A. Johnson**[‡¶2]

From the [‡]*Institute for Cellular and Molecular Biology, the* [§]*Center for Systems and Synthetic Biology, and the* [¶]*Department of Chemistry and Biochemistry, University of Texas, Austin, Texas 78712*

Background: Mutations in the human mitochondrial DNA polymerase (Pol-γ) have been linked to diseases with varying severity and age of onset.
Results: Yeast cells expressing human Pol-γ reveal a correlation of Pol-γ fidelity with human disease onset.
Conclusion: Humanized yeast provides an efficient system to correlate biochemical defects in Pol-γ with physiological consequences.
Significance: The Pol-γ-associated diseases may be caused by the low accuracy of Pol-γ mutants, not low rates of replication.

Mutations in the human mitochondrial polymerase (polymerase-γ (Pol-γ)) are associated with various mitochondrial disorders, including mitochondrial DNA (mtDNA) depletion syndrome, Alpers syndrome, and progressive external opthamalplegia. To correlate biochemically quantifiable defects resulting from point mutations in Pol-γ with their physiological consequences, we created "humanized" yeast, replacing the yeast mtDNA polymerase (MIP1) with human Pol-γ. Despite differences in the replication and repair mechanism, we show that the human polymerase efficiently complements the yeast *mip1* knockouts, suggesting common fundamental mechanisms of replication and conserved interactions between the human polymerase and other components of the replisome. We also examined the effects of four disease-related point mutations (S305R, H932Y, Y951N, and Y955C) and an exonuclease-deficient mutant (D198A/E200A). In haploid cells, each mutant results in rapid mtDNA depletion, increased mutation frequency, and mitochondrial dysfunction. Mutation frequencies measured *in vivo* equal those measured with purified enzyme *in vitro*. In heterozygous diploid cells, wild-type Pol-γ suppresses mutation-associated growth defects, but continuous growth eventually leads to aerobic respiration defects, reduced mtDNA content, and depolarized mitochondrial membranes. The severity of the Pol-γ mutant phenotype in heterozygous diploid humanized yeast correlates with the approximate age of disease onset and the severity of symptoms observed in humans.

Human mitochondria contain a 16.5-kb circular double-stranded DNA genome that encodes 13 of the proteins involved in oxidative phosphorylation. In humans, there are thousands of mitochondrial DNA (mtDNA)[3] copies per cell, so that mitochondrial genetics are complicated by heteroplasmy, the mixed population of mutant *versus* wild-type alleles. Mitochondrial DNA is replicated and repaired by the nuclearly encoded DNA polymerase (polymerase-γ (Pol-γ)), which is a heterotrimeric complex that can be reconstituted *in vitro* (1) from the 140-kDa catalytic subunit (Pol-γA) and a 55-kDa dimeric accessory subunit (Pol-γB). The catalytic subunit contains both DNA polymerase and exonuclease proofreading activities (2), whereas the accessory subunit facilitates processive DNA synthesis (1) but may also play other roles during replication. The Pol-γ holoenzyme functions in conjunction with the mitochondrial DNA helicase (3) and single-stranded DNA-binding protein (mtSSB), forming the minimal replisome (4, 5).

Mutations in *POLG* lead to clinical symptoms of varying severity, including progressive external ophthalmoplegia (PEO), Alpers syndrome, parkinsonism, and other encephalomyopathies associated with mutations, deletions, or depletions of mtDNA (6). More than 200 point mutations in the polymerase have been correlated clinically with various mitochondrial diseases (7). The effects of a small subset of these mutations on the kinetics of DNA replication have been quantified, but different models have been proposed for how changes in enzyme kinetics lead to the accumulation of mtDNA defects, ranging from low fidelity to slow rates of replication or stalling of the replisome (8–12). Moreover, many Pol-γ-associated mitochondrial disorders exhibit slow onset and a broad clinical spectrum, and the presence of the wild-type allele further complicates our ability to extrapolate from the observed biochemical defects of a mutant enzyme to a projected physiological effect (13).

* This work was supported, in whole or in part, by National Institutes of Health Grant GM044613 (to K. A. J.) and a grant from the National Institutes of Health, NIGMS (to E. M. M.). This work was also supported by Welch Foundation Grants F-1604 (to K. A. J.) and F-1515 (to E. M. M.), the National Science Foundation (to E. M. M.), the Cancer Prevention Research Institute of Texas (to E. M. M.), and United States Army Grant 58343-MA (to E. M. M.).
[S] This article contains supplemental Table S1.
[1] To whom correspondence may be addressed: Institute for Cellular and Molecular Biology, University of Texas, 2500 Speedway, Austin, TX 78712. E-mail: yufengqian1005@gmail.com.
[2] To whom correspondence may be addressed: Institute for Cellular and Molecular Biology, University of Texas, 2500 Speedway, Austin, TX 78712. E-mail: kajohnson@mail.utexas.edu.

[3] The abbreviations used are: mtDNA, mitochondrial DNA; CLS, yeast chronological life span; Pol-γ, polymerase-γ; PEO, progressive external ophthalmoplegia; Ni-NTA, nickel-nitrilotriacetic acid; MLS, mitochondrial localization sequence; qPCR, quantitative PCR; Ery[R], erythromycin-resistant.

Kinetic analysis of the effects of several point mutations on Pol-γ fidelity and efficiency of replication, combined with the structure of human Pol-γ (14), has provided molecular details regarding the primary effects of these disease-causing point mutations (8–12). For example, the mutation H932Y at the polymerase active site is associated with an autosomal recessive form of PEO and SANDO (sensory ataxic neuropathy, dysarthria, and opthalmoparesis) (15). Pre-steady state kinetic studies (8) showed that the H932Y mutation reduces the efficiency (k_{cat}/K_m) governing correct nucleotide incorporation 150-fold. Another active site mutation in Pol-γ, Y955C, was found in patients presenting "early onset autosomal dominant PEO" in their twenties (16). Kinetic analysis showed a 1300-fold reduction in k_{cat}/K_m while incorporating a dATP base opposite a template T (9, 11).

A recent study suggested that the severity of the clinical symptoms correlates with reduced rates of DNA replication by the mutant forms of the enzyme (17). However, predicting the physiological consequences of biochemical defects measured *in vitro* is complicated by the interplay of wild-type and mutant alleles and unknown adaptive control pathways and repair processes *in vivo*. Therefore, it is important to study the effects of mutations in the context of mtDNA replication in heterozygous diploid cells in order to elucidate the molecular basis of the diseases and to distinguish the consequences of various biochemical defects observed *in vitro*.

Yeast has been proposed as a suitable *in vivo* model to provide relevant information on the mechanism of human mtDNA replication because of the significant homologies in the enzymes involved (for reviews, see Refs. 18–21). Phylogenetic analysis has identified significant similarities between the DNA replication machinery of the T-odd bacteriophage and that for mtDNA replication in humans, plants, and yeast (22). Thus, evolutionary conservation and fundamental genetic similarities of mitochondria in yeast and humans make yeast a valuable tool for the investigation of mitochondrial function in normal and disease states (11, 23–28).

Previous studies (24, 27, 28) using yeast as the model to mimic human mitochondrial disease were based on the homology of yeast mitochondrial DNA polymerase (MIP1) and human Pol-γA (~65% in polymerase and exonuclease domains). These studies relied on the simple viability screen to provide a simple yes/no answer as to whether a given mutation could produce a defective phenotype consistent with the predictions from human genetic analysis (27). However, mutations in MIP1 have not been characterized biochemically, and therefore correlations rely upon untested assumptions regarding the effects of mutations on enzyme activity. Indeed, mutations in MIP1 may not cause the same changes in DNA replication rate and fidelity as their human counterparts due to subtle changes in structure and kinetics in comparing the yeast and human enzymes (1, 2, 14, 29). Therefore, the significance of studies on the physiological consequence of mutations in MIP1 may by questionable. In addition, not all important amino acid residues in human Pol-γ have yeast orthologs. In particular, yeast does not encode the homolog of accessory subunit of Pol-γ (Pol-γB), and the accessory interaction domain is not conserved in yeast. Several pathogenic point mutations are found in these domains (30, 31) in humans and cannot be tested using MIP1. Thus, despite evolutionary relationships between yeast and humans, one might question whether the human mtDNA polymerase could provide functional substitution for the yeast polymerase.

The "humanized" yeast system, with the yeast genes replaced by their human orthologs, has been developed to rapidly examine the pathology of human genetic variation, thanks to the powerful genetic tools available for yeast (32–35). Here, we begin addressing important questions by developing "humanized" yeast expressing human mitochondrial DNA polymerase genes with wild-type and mutant alleles. We show that the human Pol-γ can efficiently complement the *mip1* knockout in yeast. We take advantage of the ability to grow yeast in both haploid and diploid states to resolve the primary effects of single point mutations in Pol-γ and to investigate the complex interplay of mutant and wild-type genes within diploid cells.

The results for a series of mutations suggest that the observed clinical symptoms in humans may primarily arise from higher mtDNA mutation frequency due to the low enzyme fidelity, rather than from the slower rate of replication as suggested in prior studies (12, 17). Although more extensive studies are needed to examine this preliminary correlation, the present study establishes the utility of the humanized yeast system to rapidly assess the possible physiological consequences of point mutations thought to be correlated with human disease.

EXPERIMENTAL PROCEDURES

Yeast Strains and Media—Medium preparation, techniques for culturing, and genetic manipulations of yeast were carried out according to standard procedures (36). Synthetic dextrose (SD), synthetic glycerol (SG), rich dextrose (YPD), and rich glycerol (YPG) media were used as indicated. Unless otherwise indicated, experiments were carried out with the strain BY4741 (*MAT***a** *his3*Δ*0 leu2* Δ*0 met15* Δ*0 ura3* Δ*0*). The *MAT*$\boldsymbol{\alpha}$ type of haploid strain was generated by transformation with a centromeric plasmid *pAG-GAL-HO* expressing the HO endonuclease to initiate the mating type conversion (37). The mating type of strains was confirmed by its ability to grow on the minimal medium plate without any supplements after mating with the *MAT***a** haploid test strain (*MAT***a** *HIS1 LEU2 MET15 URA5).* The heterozygous diploid strains (*mip1*::Pol-γA Δ25 wild-type/*mip1*::hPol-γA Δ25) for all mutants studied were obtained by isolation of zygotes after 4 h of mating between the *MAT*$\boldsymbol{\alpha}$ type of haploid strain (*mip1*::hPol-γA Δ25 wild-type) with the *MAT***a** type of haploid strains (*mip1*::hPol-γA Δ25 mutants). The heterozygous diploid strains were verified by their inabilities to mate either with *MAT*a or *MAT*α haploid strain.

Humanized Yeast Strain Construction—Our method for replacement of the *MIP1* gene with the human Pol-γA (*Pol-γA*) gene is modified from the method described previously (38). Briefly, in order to generate the *mip1* knock-out haploid strain, the wild-type BY4741 strain was transformed with a PCR-amplified *Kluyveromyces lactis I-SceI-URA3* counterselectable marker cassette flanked by 60 bp of homology (primers P1 and P2; supplemental Table S1) to the yeast genomic region to be disrupted (Fig. 1 and supplemental Table S1). The disruption of the *MIP1* gene was done so that the native yeast mitochondrial localization signal sequence was retained at the N terminus of

the gene along with the promoter. Primers (P3 and P4; supplemental Table S1) binding to the yeast genome ~200 bp outside of the homology region were used to confirm the knockout of the *mip1* gene and were also used for verification by DNA sequencing. The Δ*mip1* strain was then transformed with plasmid *pGAL1-I-SceI-G418* expressing an I-SceI endonuclease under the *Gal* promoter. To create a double-stranded break at the target site, overnight-grown cells in YPD medium were diluted into YEP-raffinose to 0.5×10^6 cells/ml and allowed to grow for 6 h at 30 °C to derepress the GAL1 promoter. Galactose was added at 1.5% final concentration in the growth medium to induce the expression of I-SceI for 1 h. Cells were pelleted for high efficiency transformation with a linear DNA amplified by PCR encoding the human Pol-γA gene with 60-bp homology as chosen earlier for disruption of the *MIP1* locus. The PCR (primers P5 and P6; supplemental Table S1)-amplified *POLGA* fragment has a 25-amino acid N-terminal deletion encoding a human mitochondrial targeting sequence (Pol-γA Δ25). The transformants were first plated on YPD-agar and allowed to grow overnight followed by replica-plating onto 5-fluoroorotic acid-agar plates to select for the loss of the URA cassette. PCR (primers P1 and P2) was carried out to check whether the URA^- transformants were due to precise replacement of the URA marker cassette with the human gene or only to removal of the URA cassette (Fig. 1).

Plasmid Construction—Site-directed mutagenesis of *Pol-γA* was performed using the QuikChange site-directed mutagenesis kit (Invitrogen) cloned in a pUC19 plasmid. The mutations were verified by DNA sequencing. The *POLGB* encoding the accessory subunit of human Pol-γ was obtained the human ORFeome collection in the form of an entry clone, pDONR223-*POLGB*. PCR using primers (P7, P8, and P9; supplemental Table S1) was used to replace the human mitochondrial localization sequence (MLS) of *POLGB* with the yeast MLS. The engineered *POLGB* carrying the yeast MLS was then TOPO-cloned into an entry clone vector, *pENTR*, followed by integrating the gene into the yeast destination vector *pAG415Gal-ccdB* under the Gal promoter or into the vector pAG*416GPD-ccdB* under the constitutive glyceraldehyde-3-phosphate dehydrogenase (GPD) promoter using the LR reaction (Gateway Technology).

Mitochondria Isolation, Co- immunoprecipitation, and Western Blots—Mitochondrial and non-mitochondrial fractions were collected with the yeast mitochondrial isolation kit MITOISO3 (Sigma-Aldrich) following the standard procedures provided by the manufacturer. The protein content was measured by Bradford assay. A total of 100 μg of the protein was loaded into wells of a 10% polyacrylamide gel and transferred into a nitrocellulose membrane. Western blotting was carried out using a 1:2000 dilution of horseradish peroxide-conjugated anti-His_6 tag as the primary antibody. Tetramethylbenzidine substrate was used for visualization of antibody-bound protein bands.

For Ni-NTA-agarose co-immunoprecipitation experiments, 2 mg of mitochondria were solubilized in buffer containing 20 mM Tris, pH 7.5, 100 mM potassium acetate, 10% (v/v) glycerol, and 2% digitonin (w/v). The supernatants were incubated with 100 μl of Ni-NTA-agarose resins for 1 h at 4 °C, beads were washed, and bound proteins were eluted with elution buffer containing 250 mM imidazole. Samples were analyzed by SDS-PAGE and immunoblotting.

Growth Curve Measurement and Analysis—The cell growth was monitored at an absorption of 600 nm on the microplate reader (BioTek Instruments, Winooski, VT). Unless otherwise indicated, cells were seeded to 96-well plates at 1×10^5 cells/ml/well in the 150-μl culture and grown at 30 °C with continuous shaking. For cultures grown with glucose as the sole carbon source, doubling time during the exponential phase of growth before or after diauxic shift was calculated from the slope of the linear increase of the natural log of cell numbers. The lag time was estimated from the intersection of two linear fits of the time course. For cultures grown in conditions other than glucose as the carbon source, the growth curve was modeled as the initial lag phase followed by the exponential phase before the cells enter the stationary phase. To mimic chemostat conditions, cells were maintained in early exponential phase by successive dilution with fresh medium. Cells were allowed to grow until an A_{600} of 0.2 and were diluted 10-fold into fresh medium. This process was repeated at least 6–8 times.

Measurement of Petite Frequency, Mutation Frequency, and mtDNA Contents—Measurement of petite frequency and erythromycin-resistant (Ery^R) mutant frequency of strains harboring Pol-γ or Pol-γ mutant alleles was carried out based on the method described previously (27). The mtDNA contents were quantified relative to nuclear DNA contents using real-time quantitative PCR. Primers and probes were designed to specifically amplify mitochondrial encoded *COX3* gene (P10 and P11; supplemental Table S1) and nuclearly encoded *GAL4* gene (P12 and P13; supplemental Table S1). PCRs and data analysis were performed as described previously (39).

Confocal Microscopy—Confocal microscopy imaging was performed on a Zeiss LSM 510 laser-scanning microscope (Carl Zeiss Inc., Thornwood, NY). To visualize mitochondria, cells harvested from different conditions (Fig. 7*A*) were washed with water and resuspended in PBS buffer with 1 mM Ca^{2+} and 0.5 mM Mg^{2+} containing 100 nM MitoTracker-Red (Invitrogen) and 1 μg/ml DAPI (Invitrogen). Cells were stained at room temperature with shaking for 30 min and then washed three times with PBS. Stained cells were mounted directly on microscope slides and examined by confocal microscopy.

Chronological Life Span Measurement—The cell viability assay was modified from the method described previously (40). Briefly, cells of each strain were grown in liquid SD medium in flasks at 30 °C with shaking (250 rpm) to ensure aeration. Cells entered stationary phase after ~48 h, when the majority of cells stop dividing. Every 2 days, aliquots from the cultures were diluted accordingly and plated (200–300 cells) onto solid SD medium plates. The plates were incubated at 30 °C for 2 days, and the viability of each strain in the flask was measured as cfu. Viability at day 3 was considered to be the initial survival (100%), and day 3 was set to be time 0.

Measurement of Δψ*m*—To measure the membrane potential change of yeast cells, we used the fluorescent carbocyanine dye JC-1 (Invitrogen) to label the mitochondria membrane following the staining procedure provided by the manufacturer. Briefly, cells were harvested at times Fig. 7*C* legends, resuspended in 1 ml of PBS containing 5 μM JC-1 probe, and

incubated for 30 min at room temperature in the dark. Cells were then washed once in PBS and analyzed immediately by flow cytometry. Control cells with depolarized mitochondrial membranes were treated with 5 μM carbonyl cyanide *m*-chlorophenyl hydrazone (Sigma-Aldrich) for 30 min at room temperature before JC-1 labeling. Photomultiplier settings were adjusted to detect red fluorescence (λ_{em} = 590 nm) of JC-1 aggregates at channels FL-1 and green fluorescence (λ_{em} = 529 nm) of JC-1 monomer at channels FL-2.

Protein Purification—Wild-type and mutant Pol-γA were expressed in insect cells and purified to homogeneity as described previously (8). Pol-γB was expressed in *Escherichia coli* and purified to homogeneity as described (1).

Nucleotide Incorporation Assays—Single nucleotide incorporation assays were performed with a RQF-3 rapid quench flow apparatus (KinTek Corp.) as described (9). In brief, 100 nM Pol-γ *exo*$^+$ enzyme was preincubated with 50 nM 5′-^{32}P-labeled DNA template (25-mer/45-mer duplex) on ice for 10 min, and the complex was rapidly mixed with 12.5 mM Mg^{2+} and 50 μM dATP for variable time at 37 °C before the reaction was quenched by mixing with 250 mM EDTA. The products were resolved on a 15% denaturing polyacrylamide sequencing gel, and then the dried gel was exposed to a phosphor screen (Molecular Dynamics). Radioactive bands were detected with a Typhoon 9400 scanner (GE Healthcare) and quantified with ImageQuant software (GE Healthcare). The data have been fit globally using the KinTek Explore program (Kin-Tek Corp.) to Scheme 1, and kinetic parameters k_{cat} and k_{cat}/K_m were derived for Scheme 1 by the simple relationship $k_{cat} = k_{pol}$ and $K_m = K_{d,app}$.

where ED_{25} represents a preformed complex of enzyme with 25/45 duplex DNA. Ground state nucleotide (N) binding is represented by the term $K_{d,app}$, whereas the chemistry step to form the complex of enzyme with 26/45 duplex (ED_{26}) and pyrophosphate (PP_i) is irreversible and described by k_{pol}.

$$ED_{25} + N \underset{}{\overset{K_{d,app}}{\rightleftharpoons}} ED_{25}N \xrightarrow{k_{pol}} ED_{26} + PP_i$$

SCHEME 1

Excision Reactions—Enzyme *exo*$^+$ (100 nM) was preincubated with 75 nM DNA. The reaction was initiated by mixing it with Mg^{2+} for variable time at 37 °C and was quenched by mixing with 250 mM EDTA. The loss of full-length substrate primer due to exonuclease digestion was plotted against time and fit to a single or double exponential indicated in the Fig. 4 legend.

RESULTS

The Human Pol-γA Complements Loss of Saccharomyces cerevisiae MIP1—The yeast nuclear *MIP1* gene encodes the mtDNA polymerase. A Δ*mip1* deletion mutant is respiration-deficient but is able to obtain energy to sustain growth from glycolysis when provided an appropriate carbon source. We took advantage of this conditional phenotype to enable replacement of the *MIP1* gene with a *Ura3*$^+$ marker cassette containing an *I-Sce1* endonuclease site while still retaining the upstream sequence encoding the MLS (Fig. 1) (see "Experimental Procedures"). The marker cassette was then replaced chromosomally by the human *POLGA* wild-type (or mutant) gene fused to the yeast MLS encoding gene fragment.

To examine whether the human *POLGA* could functionally substitute *MIP1* in *S. cerevisiae*, we first assayed the localization of the human Pol-γA protein by immunofluorescence using anti-His_6 antibodies. The Pol-γA protein was detected in the purified mitochondrial fraction (Fig. 2*A*), indicating that the human Pol-γA protein was expressed and successfully targeted to mitochondria by the yeast MLS. We then compared growth curves of the humanized and wild-type strains. In haploid cells, a deletion of *mip1* resulted in an inviable strain when grown in synthetic medium with 2% galactose as the carbon source (Fig. 2*B*) and formed 100% petite colonies when grown in glucose medium (Table 1 and Fig. 2*C*). The human gene rescued the petite phenotype of the Δ*mip1* strain (Table 1 and Fig. 2*C*). These strains can metabolize galactose to sustain growth with a doubling time of 3.2 ± 0.02 h, which is only slightly less than that of the wild-type strain (2 ± 0.3 h). However, growth of the *POLGA* strain showed a longer lag time of 18 ± 1.1 h, as opposed to the wild-type strain (7.2 ± 0.2 h) in recovering from stationary phase.

Pol-γB Is Required for Complete Complementation—We sought to investigate whether the inefficient complementation was due to the absence of the human accessory protein Pol-γB. *In vitro* studies have shown that Pol-γB forms a stable protein complex in its dimeric state with Pol-γA (41), stimulates DNA binding to Pol-γ by 3.5-fold, and increases the polymerization rate by 4.5-fold (1). We expressed human Pol-γB fused to the MIP1 MLS in yeast cells using a CEN plasmid, *pAG415GAL-POLGB*, under the control of a *GAL*-inducible promoter. The empty plasmid was used as the negative control. As shown in Fig. 2*B*, expression of Pol-γB in the Pol-γA-expressing strain dramatically shortened the lag time from 18 h to 6.9 h and slightly increased the growth rate. Surprisingly, in the presence of human Pol-γB, the wild-type strain expressing yeast MIP1 grows at a rate that is comparable with that seen with Pol-γA (Fig. 2*B*). Thus, when one takes into account a slight inhibition of grown caused by expressing Pol-γB, the human Pol-γA appears to efficiently complement the *mip1* knockouts.

The interaction of the Pol-γA with Pol-γB *in vivo* was analyzed with mitochondrial extracts from cells expressing Pol-γA with His_6 tag and Pol-γB (Fig. 2*D*). When mitochondrial extracts containing Pol-γA-His_6 were pulled down by Ni-NTA, we detected a large portion of Pol-γB (52 kDa band) co-immunoprecipitated with Pol-γA-His_6. Control experiments using mitochondrial extracts from cells expressing Pol-γB only showed that Pol-γB was not retained by Ni-NTA. Likewise, the 52-kDa protein was absent in the mitochondrial extracts from cells expressing Pol-γA-His_6 only. The results demonstrate the specificity of the interaction between Pol-γA with Pol-γB in the cell.

To further examine the functional complementation of *mip1* deletion by human *POLG*, we measured the mtDNA content and mtDNA mutation frequency. The relative mtDNA content was measured using qPCR by comparing the ratio of copy numbers of the mitochondrially encoded *COX3* gene to the nuclearly encoded *GAL4* gene, as described previously (39). Compared with wild-type strains, the *POLGA* haploid strain contained about 30%

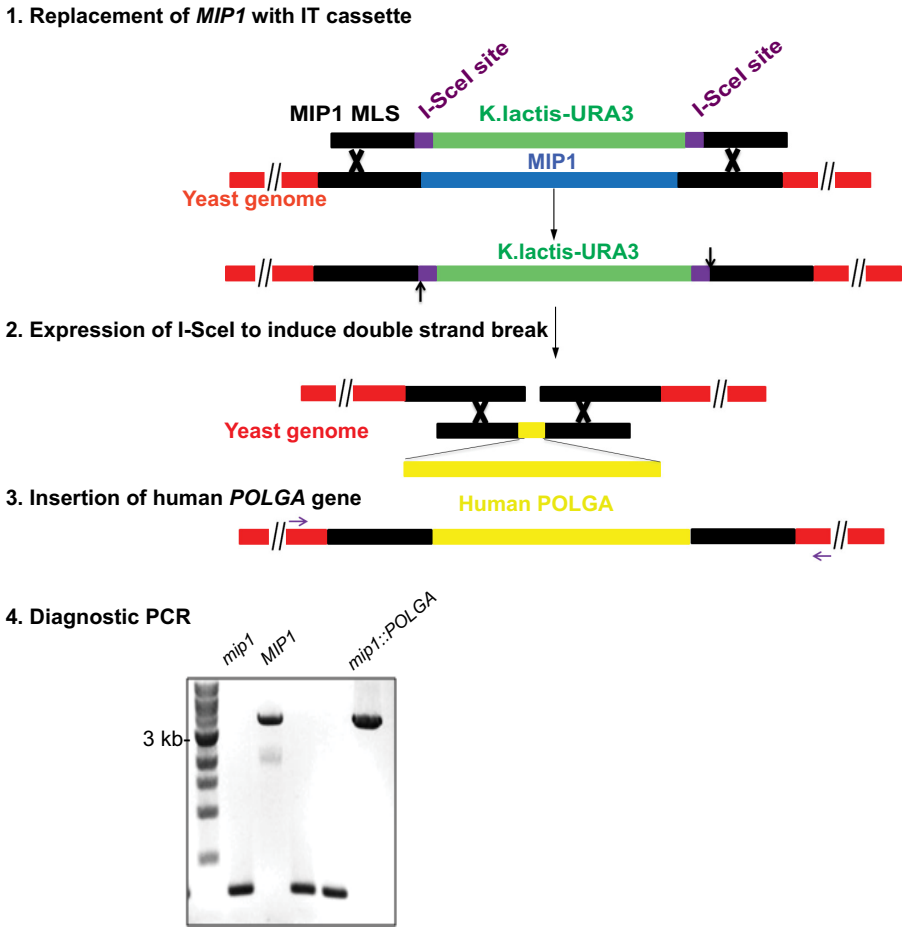

FIGURE 1. **Replacement of nuclear *MIP1* gene from *S. cerevisiae* with the human *POLGA* gene.** All of the strains were verified by PCR using primers outside the region of disruption followed by DNA sequencing.

of the mtDNA during the exponential growth phase; this value increased to about 52% when Pol-γB was also present (Fig. 3*C*).

The frequency of mtDNA mutation was assayed by selecting for resistance to erythromycin (Ery^R), which is conferred by point mutations in the mtDNA-encoded 21 S rRNA gene (42). There are no reported nuclear mutations in yeast that result in Ery^R; therefore, the frequency of Ery^R can be used to estimate the frequency of mtDNA mutation. The *POLG* haploid cells showed no significant increase in mutation frequency compared with the *MIP1(WT)* haploid cells (Table 1). We next directly visualized mitochondria using confocal microscopy by staining nuclear and mitochondrial DNA by DAPI and mitochondria using MitoTracker Red. As shown in Fig. 3*E*, both mtDNA and functional mitochondria were retained in haploid cells expressing human Pol-γ, further supporting the functional complementation of *mip1* by the human *POLG* gene.

Mutations in Pol-γ Cause Oxidative Growth Defects in Haploid Yeast Cells—Using the humanized yeast model, we can now evaluate the effects of specific disease-associated point mutations in human Pol-γ *in vivo*. The mutations considered in this study and their associated diseases are listed in Table 1. We assayed several features for each mutant: oxidative growth phenotype, mtDNA content, mitochondrial function, petite phenotype percentage, and mtDNA mutation frequency (Ery^R phenotype). As shown in Fig. 3*A*, all six mutants except the Δ*mip1* strain showed similar doubling times in the initial exponential growth phase on glucose, where ATP is primarily generated by glycolysis. After the diauxic shift, when cells are required to obtain energy from aerobic respiration, no apparent growth was observed for any of the mutant strains compared with the wild-type *POLG* exo^+ strain (which showed a doubling time of 37 h).

To provide a direct test of mitochondrial function, cells were grown on glycerol, a non-fermentable carbon source. Of the six mutant haploid strains, five strains (*S305R*, *H932Y*, *Y951N*, *Y955C*, and Δ*mip1*) were unable to grow on glycerol (Fig. 3*B*), whereas the exonuclease-deficient (exo^-) strain grew poorly on glycerol (Fig. 3*B*) with doubling times of 21 h, compared with 4.5 h for wild-type Pol-γ exo^+. The maximum cell densities obtained with exo^- mutant, determined by A_{600}, were dramatically lower than that of the wild-type exo^+ strain (Fig. 3*B*). Moreover, all mutant haploid showed significantly increased frequencies of petite formation compared with the Pol-γ exo^+ wild-type strain (Table 1).

Oxidative Growth Deficiency Is Associated with mtDNA Depletion and Mutation in Haploid Cells Harboring Mutant Pol-γ—Because mtDNA depletion is a common feature of Pol-γ-related diseases, we hypothesized that Pol-γ mutant strains would lead to decreased mtDNA content. To measure mtDNA copy number, we performed real-time qPCR to quantify mito-

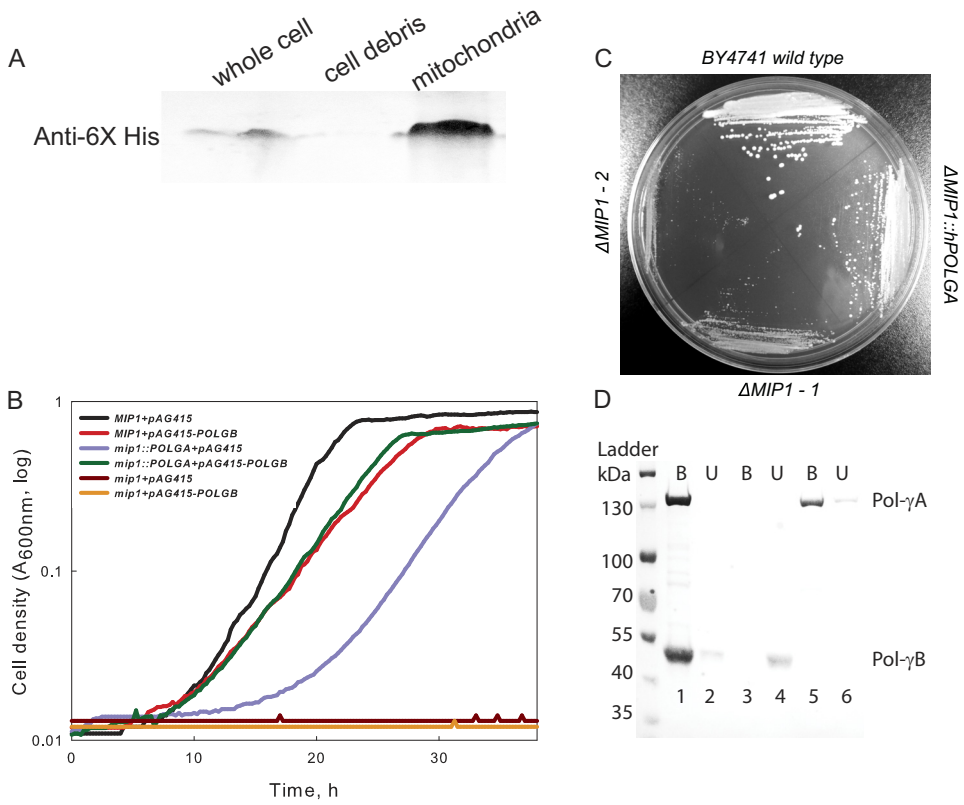

FIGURE 2. **The human polymerase γ complement *mip1* deletion in *S. cerevisiae*.** *A*, Western blot analysis of the localization of Pol-γA. Mitochondrial extracts were purified from *mip1*::*Pol-γ* haploid cells growing in the exponential phase on glycerol. HRP-conjugated-anti-His_6 antibodies (Abs) recognize a 130 kDa band in whole cells (*lane 1*) and in the mitochondrial fraction (*lane 3*). *B*, complementation of MIP1 by Pol-γA in the presence or absence of Pol-γB. Haploid cells carrying either empty plasmid *pAG415Gal* or *pAG415Gal-POLGB* were grown at 30 °C on SC medium supplemented with 2% galactose. The data are representative of at least three independent experiments. *C*, the human *POLGA* gene rescued the petite phenotype of the Δ*mip1* strain. Haploid cells were streaked on YPD solid medium and incubated in 30 °C for 2 days. *D*, mitochondrial extracts were isolated from haploid cells carrying Pol-γA^+ *GPD416*-Pol-γB (*lanes 1* and *2*), MIP1$^+$ *GPD416*-Pol-γB (*lanes 3* and *4*), or Pol-γA (*lanes 5* and *6*). Solubilized mitochondria were incubated with Ni-NTA resin for 1 h at 4 °C. After elution with imidazole-containing buffer, proteins were analyzed by SDS-PAGE and Western blotting using a combination of anti-His_6 tag and anti-Pol-γB Abs (*lanes 1* and *2*), anti-Pol-γB Abs (*lanes 3* and *4*), or anti-His_6 tag Abs (*lanes 5* and *6*). *U*, mitochondrial fractions unbound to Ni-NTA resin. *B*, material bound to Ni-NTA resin.

TABLE 1

Summary of petite formation and mutant frequency in all studied strains

Mutation	Disease	Percentage petite (haploid)	Percentage petite (diploid)	Ery^R frequency (haploid)	Ery^R frequency (diploid)
		%	%	$\times 10^{-7}$	$\times 10^{-7}$
MIP1 *WT*		3.5 ± 0.3	0.5 ± 0.2	1.1 ± 0.2	ND[a]
POLG *WT*		8 ± 0.2	1.1 ± 0.3	2.5 ± 0.2	1.5 ± 0.2
POLG *exo*$^-$	Premature aging[b]	48 ± 5	4.2 ± 1.2	172 ± 7.1	52 ± 5
POLG *S305R*	Alpers	100	3.1 ± 0.3	ND	11 ± 2
POLG *H932Y*	PEO, SANDO	100	12 ± 1.2	ND	86.6 ± 12
POLG *Y951N*	Peripheral neuropathy	100	16 ± 2	ND	14 ± 1.7
POLG *Y955C*	PEO	100	24 ± 4.2	ND	35.3 ± 2.4
Δ*mip1*		100	2.4 ± 0.9	ND	3.2 ± 0.8

[a] ND, not determined.
[b] Studies were done in mice (50, 51).

chondrial genes in total DNA extractions from haploid mutant strains. In all strains, large increases in petite frequency were correlated with significant decrease or total depletion of mtDNA (Fig. 3*C*).

We also examined the effects of mutations in Pol-γ on haploid strains by confocal fluorescence microscopy following DAPI staining of both nuclear and mtDNA and MitoTracker Red staining of mitochondria. In haploid strains, mtDNA was detected in the wild-type Pol-γ and *exo*$^-$ cells (Fig. 3*E*). However, no apparent mtDNA staining could be observed in the cells harboring *S305R*, *H932Y*, *Y951N*, or *Y955C* mutations in Pol-γ. Consistent with mtDNA depletion, no functional mitochondria were observed in these cells. Although we have not tested the effects of *POLG* mutations on nuclear DNA replication as measured by *GAL4* gene levels, the data clearly show a selective reduction in mtDNA replication relative to nuclear DNA.

The haploid cells carrying exonuclease deficient Pol-γ (*exo*$^-$) showed the largest increase (Table 1) in the Ery^R mutation frequency, supporting the significant role of proofreading activity of Pol-γ in mtDNA maintenance. DNA sequencing analysis of the cloned 21 S rRNA gene (primers P14 and P15; supplemental Table S1) from Ery^R resistant

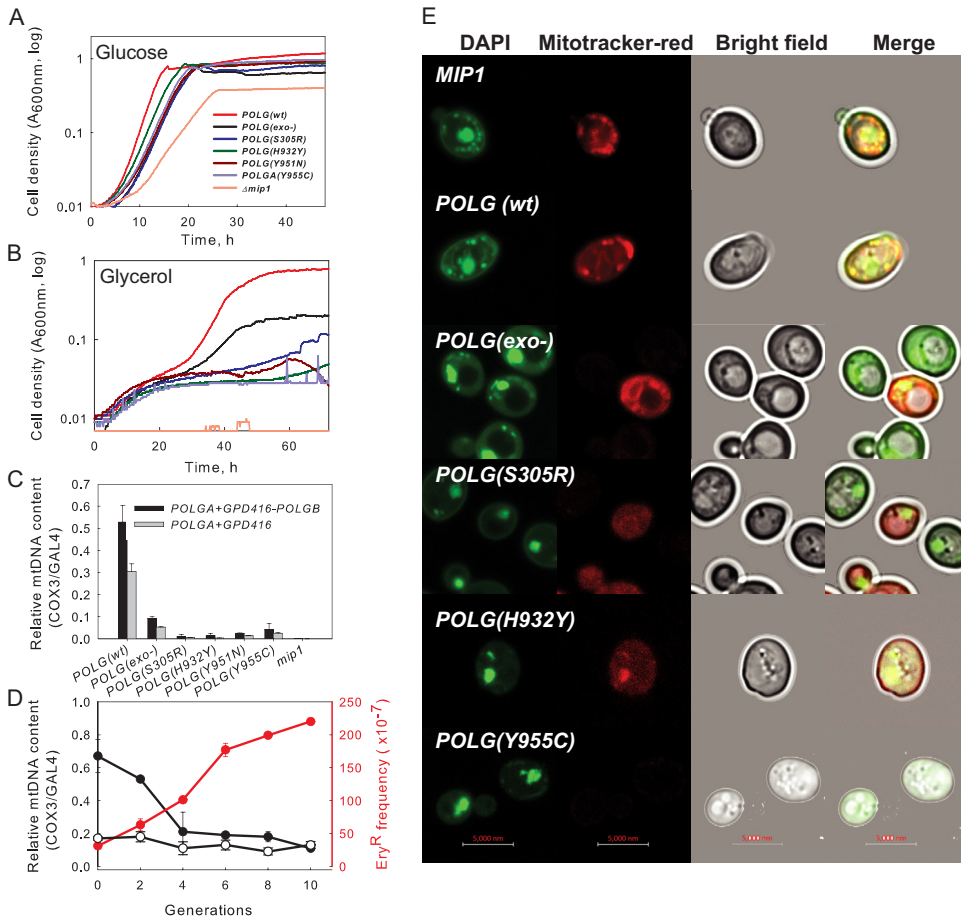

FIGURE 3. **Oxidative growth phenotypes of haploid strains (*mip1*::*POLGA* + *POLGB*) harboring the indicated point mutants.** Shown are growth curves of haploid cells in synthetic medium without uracil (−ura) supplemented with 2% D-glucose (*A*) or 2.5% glycerol (*B*). *C*, normalized relative mtDNA content of haploid cells in the presence (*black bar*) or absence (*gray bar*) of Pol-γB. Genomic DNA was extracted from cells growing in the exponential phase on 2% dextrose (OD = 0.4). The copy number of the mitochondria *COX3* gene relative to that of the nuclear *GAL4* gene by qPCR was normalized to 1 for wild-type MIP1 cells. *Error bars*, S.D. values of triplicate PCRs. *D*, generation dependence of mtDNA contents and Ery^R frequency for *Pol-γ*-exo$^-$ (*filled circle*) and *Pol-γ*-Y955C haploid (*open circle*) cells. The cells were continuously grown in SD liquid medium (−ura) and maintained in exponential growth phase by successive dilutions to fresh medium (see "Experimental Procedures" for details). Aliquots were taken at the indicated time to measure the relative mtDNA contents using qPCR as described above or to determine the Ery^R mutant frequency (*red symbols*) following methods described previously (27). The ratio of *COX3/GAL4* was normalized to 1 for wild-type Pol-γ cells. *E*, representative confocal microscopy images of haploid cells with mitochondria stained with MitoTracker Red and DNA stained with DAPI. The DAPI-stained mtDNA was revealed by a network of punctuate dots located at the cell periphery for wild-type MIP1, wild-type *Pol-γ*-exo$^+$, and *Pol-γ-exo*$^-$ cells. The *green spots* present in the cytoplasm are nuclear DNA. For *Pol-γ*-S305R, *Pol-γ*-H932Y, and *Pol-γ*-Y955C cells, MitoTracker Red diffused in the cytoplasm, suggesting loss of functional mitochondria.

exo$^-$ cells mapped mutations at nucleotide position 1951 (A to T, A to G, A to C, and a single G insertion between 1950 and 1951). The Pol-γ showed an average discrimination factor of 3×10^5 against mismatched nucleotides, which equals a mutation rate of 3.3×10^{-6}/nucleotide/genome replication in the absence of the proofreading activity (8, 9). In accordance with *in vitro* measurements, the mutation rate of *exo*$^-$ cells after ~4–5 generations is 1.7×10^{-5} (Table 1). The mutation rate increased over time by maintaining the cells in exponential growth phase (Fig. 3*D*), and accumulated mtDNA mutation may lead to the observed decrease in mtDNA contents (Fig. 3*D*).

Oxidative Growth Deficiency of Haploid Cells Is Correlated with the Low Fidelity of Pol-γ Mutants—The haploid strains carrying H932Y, Y951N, or Y955C mutations form 100% petite cells (Table 1). Kinetic analysis of purified Pol-γ mutants showed a ~150-, 11-, and 1300-fold decrease in the rate of dATP incorporation for H932Y, Y951N, and Y955C, respectively, compared with the wild-type enzyme (1, 8, 9).[4] Strikingly, the fidelity of Pol-γ mutants as calculated from the ratio of k_{cat}/K_m values for correct (dATP:dT) *versus* mismatched (TTP:dT) base pairs dropped ~100-fold for Y955C and ~3-fold for H932Y (8, 9). Moreover, unlike wild-type enzyme, both H932Y and Y955C mutants can quickly incorporate multiple mismatched base pairs *in vitro*, suggesting the importance of enzyme fidelity and the ability of the enzyme to sense and remove mismatched base pairs (8, 9).

The S305R haploid cells are not viable in glycerol medium, which requires oxidative metabolism for use as a carbon source. For the purified S305R Pol-γ, quenched-flow analysis of correct base incorporation yielded values for k_{cat} and K_m of ~8 s^{-1} and 0.7 μM, respectively (Fig. 4*A*), which results in only a ~3-fold decrease in k_{cat}/K_m compared with the wild-type enzyme

[4] D. Batabyal, J. L. Ziehr, and K. A. Johnson, manuscript in preparation.

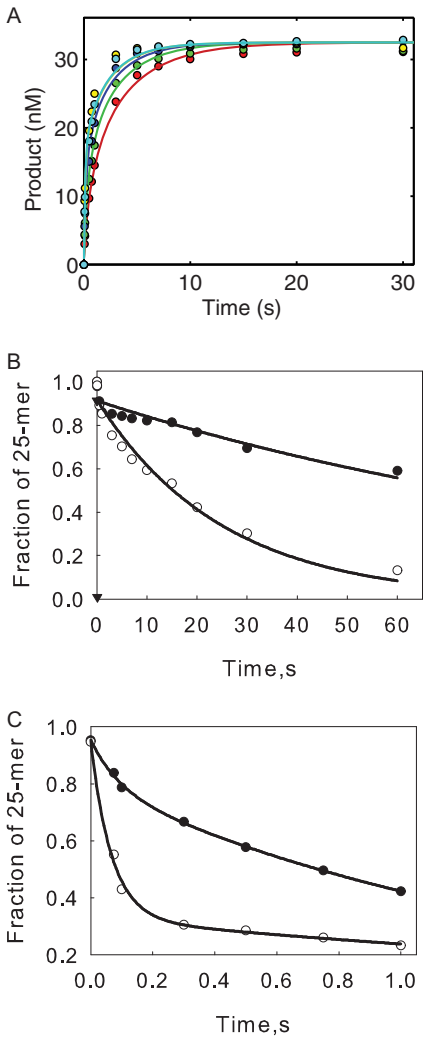

FIGURE 4. **Kinetic characterization of S305R mutant.** *A*, kinetic incorporation of dATP for S305R mutant. For each concentration series, a preformed enzyme-DNA complex ([enzyme] > [DNA duplex]) was mixed with variable concentrations of nucleotide (0.25, 0.4, 1, 6, and 17 μM) and then quenched with 0.5 M EDTA. In each *panel*, the *smooth lines* represent the best fit to the model shown in Scheme 1 using KinTek Explore software. The fit yielded a k_{pol} of 8.23 ± 2 s^{-1} and a $k_{d,app}$ of 0.7 ± 0.15 μM. *B*, excision of single-stranded DNA for WT (○) and S305R mutant (●). Enzyme (100 nM) was preincubated with 75 nM single-stranded 25-mer DNA, and the cleavage reaction was initiated by adding Mg^{2+} and excess unlabeled 25-mer DNA trap. The percentage of 25-mer remaining was plotted against reaction time and fit to a single exponential to yield an excision rate of 0.03 ± 0.005 s^{-1} for WT enzyme and 0.008 ± 0.0009 s^{-1} for the S305R enzyme, respectively. *C*, excision of DNA containing four mismatches. Enzyme (100 nM) was preincubated with 75 nM 25/45 DNA containing four mismatches (DNA sequence shown in supplemental Table S1), and Mg^{2+} was added to initiate the excision reaction. The percentage of 25-mer remaining was plotted against time and fit to a double exponential to yield a fast excision rate of 15.4 ± 1.1 s^{-1} for WT enzyme (○) and 5.5 ± 0.7 s^{-1} for S305R enzyme (●).

($k_{cat}/K_m = 40\ \mu M^{-1}\ s^{-1}$). It is unlikely that this small reduction of the replication rate would lead to the complete loss of functional mitochondria. Because the Ser-305 residue is located near the partitioning loop between the polymerization active site and exonuclease active site, we next examined the proofreading activity by S305R Pol-γ. Compared with the wild-type enzyme, the S305R mutant showed a 10-fold reduction in the rate of excision of single-stranded DNA and a ~3-fold decrease in the rate of excision of mismatched base pairs (Fig. 4, *B* and *C*). Therefore, the deficiency of proofreading activity coupled with the slow replication rate by S305R Pol-γ could account for the oxidative growth defect of *S305R* haploid cells.

Collectively, each mutation that we examined presents a severe defect in mtDNA replication in haploid yeast cells, consistent with the observation that these mutations are never observed in the homozygous state in humans, presumably due to the lethality of the mutations. We next examined the effect of these mutations in the diploid heterozygous cells expressing one wild-type and one mutant gene.

Heterozygous Diploid Cells Mimic the Compound Heterozygotes of Human Pol-γ Mutations—We generated heterozygous diploid strains of yeast by mating ancestor haploid cells harboring the wild-type *POLG* gene with ones harboring mutant *POLG* gene. The Pol-γB is always co-expressed in all heterozygous diploid cells under the constitutive GPD promoter. The doubling times of cells grown on glucose are quite similar for all heterozygous mutants in their initial exponential growth phase (Fig. 5*A*), although the mutants differed in growth rates after the diauxic shift.

To directly monitor the respiratory function of the heterozygous diploid mutant strains, cells were grown on glycerol. As shown in Fig. 5*B*, the mutant strains started out with the same growth rate as the wild-type strains until the OD reached ~0.4, when most mutants began to grow much more slowly than the wild-type strain. Interestingly, the heterozygous strain (*POLG* WT/*mip1*) grew with the same doubling time as the wild-type cells (*POLG* WT/*POLG* WT) although it showed a longer lag time (Fig. 5*B*), suggesting a possible underlying mechanism to control mtDNA copy number.

In the heterozygous diploid strains, qPCR analysis of the mtDNA content indicated that mtDNA was retained to different extents, but all mutant strains grown in the early exponential phase still retained >50% relative to the *POLG(WT)/POLG(WT)* diploid strain (Fig. 5*C*). Consistent with the qPCR results, we also detected the presence of DAPI-stained mtDNA in all heterozygous mutant cells (Fig. 5*D*), indicating that the wild-type Pol-γ is able to efficiently replicate the mtDNA to maintain the functional mitochondria initially. Thus, deficiencies in rates of polymerization by the mutant forms of Pol-γ may not contribute significantly to the observed mtDNA depletion. Rather, the wild-type enzyme appears to compensate for deficiencies in the rates of replication catalyzed by the mutant forms of the enzyme in heterozygous cells.

Long Term Growth in Chemostatic Conditions Leads to Accumulation of Mitochondrial Damage in Heterozygous Mutant Diploid Cells—All mutant heterozygous diploid cells showed a growth deficiency after the cultures reached an A_{600} greater than 0.4. We propose that this phenomenon may indicate that the mtDNA replication is eventually impaired by the accumulation of mutations deriving from the mutant Pol-γ. However, interpreting the changes in growth rate is complicated by the complex nutrient changes occurring in the medium as the cultures approach stationary phase. Therefore, to test our hypothesis, we performed a continuous growth experiment by maintaining the cells in exponential growth phase for several days (see "Experimental Procedures" for details). This was accomplished by successive dilutions of cultures into fresh medium; when each culture reached an A_{600} of >0.2, it was diluted by the addition of fresh medium to an A_{600} of 0.02 to begin a new

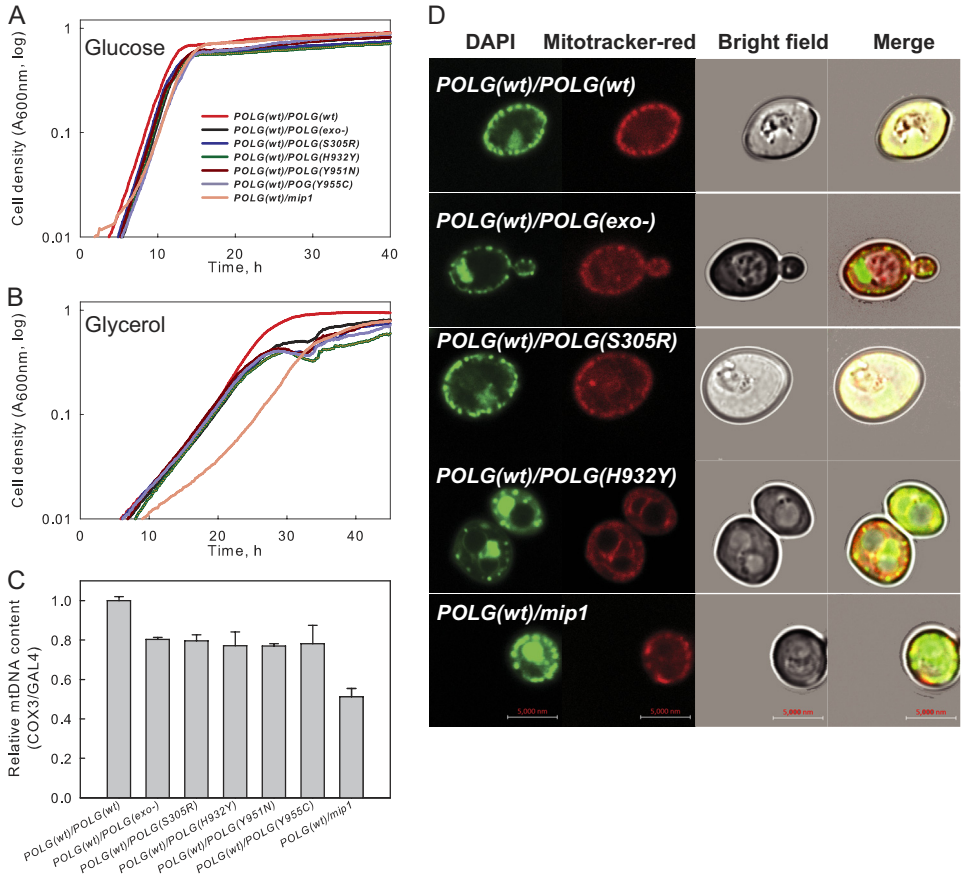

FIGURE 5. **Oxidative growth phenotypes of heterozygous diploid strains (*POLG(WT)*/*polg*) harboring the point mutation as described.** Shown is growth curve measurement of heterozygous diploid cells grown in synthetic medium without uracil supplemented with 2% dextrose (*A*) or 2.5% glycerol (*B*). *C*, relative mtDNA contents of heterozygous diploid strains as measured by qPCR. Genomic DNA was extracted from cells growing in the exponential phase on 2% dextrose (OD = 0.4). The *COX3*/*GAL4* ratio by qPCR was normalized to 1 for the *POLG(WT)*/*POLG(WT)*. *D*, representative confocal microscopy images of heterozygous diploid cells stained with MitoTracker Red and DAPI. *Error bars*, S.D.

growth phase (Fig. 6*A*). We reasoned that by avoiding shifts in metabolism due to changes in the medium, the observed growth defects should reflect intrinsic imparities in mtDNA replication. As shown in Fig. 6*A*, after 40 h of continuous growth (one dilution cycle) and ~10 generations from the ancestor, the *Y955C* and *Y951N* heterozygous diploid strains began to grow notably more slowly than the wild-type cells. After ~30 generations, all heterozygous diploid mutant cells showed growth deficiencies on glycerol. The doubling times of all mutants for each round of growth are summarized in Fig. 6*B*, demonstrating the early onset of growth defect for Y995C and Y951N heterozygous diploid strains.

To understand the molecular basis for this oxidative growth phenotype, we measured the mtDNA content of cells from different generations (Fig. 6*C*). For heterozygous diploid cells (*exo*$^-$, *H932Y*, *Y955C*, and *Y951N*), mtDNA content reduced with successive generations; nonetheless, levels of mtDNA remained above 30% relative to the wild-type Pol-γ strain even after 30 generations, indicating that mtDNA depletion may not be the only factor leading to the slower growth rate.

Onset of Growth Defects Is Associated with Mitochondrial Membrane Depolarization—For *Y955C* mutants, we observed dramatically decreased fluorescence from MitoTracker Red-labeled mitochondria with successive generations (Fig. 7*A*), possibly suggesting mitochondrial membrane depolarization because MitoTracker Red accumulation depends upon a functional mitochondrial membrane potential. To test this idea, we labeled the cells with JC-1, which undergoes an emission spectrum change from 590 nm (JC-1 aggregates) to 530 nm (JC-1 monomer) upon membrane depolarization. Ratiometric measurements of the red (monitored at FL-1 channel) to green (monitored at FL-2 channel) JC-1 fluorescence indicate $\Delta\psi m$ (44). Flow cytometry (Fig. 7*B*) revealed a progressive population shift of cells with high fluorescence intensity in the FL-1 channel toward low fluorescence intensity as a function of the cell generations for *Y955C* heterozygous diploid strains, consistent with our observations by confocal microscopy (Fig. 7*A*). We performed similar experiments for other heterozygous diploid mutants and have plotted the relative change of mean FL-1 fluorescence for each heterozygous diploid mutant at different generations, as shown in Fig. 7*C*. The Pol-γ *Y955C*, *Y951N*, and *exo*$^-$ mutants showed more rapid decline in $\Delta\psi m$ compared with other mutants, which is correlated with a higher mutation frequency of these mutants and precedes the reduction in mtDNA content (Fig. 6*C*).

Mutation Rates Correlate with the Chronological Life Spans of Mutants—Most mitochondrial diseases affect postmitotic cells, and disease progression is characterized by delayed onset. The yeast chronological life span (CLS) is defined as the length of time that a non-dividing yeast cell survives in stationary

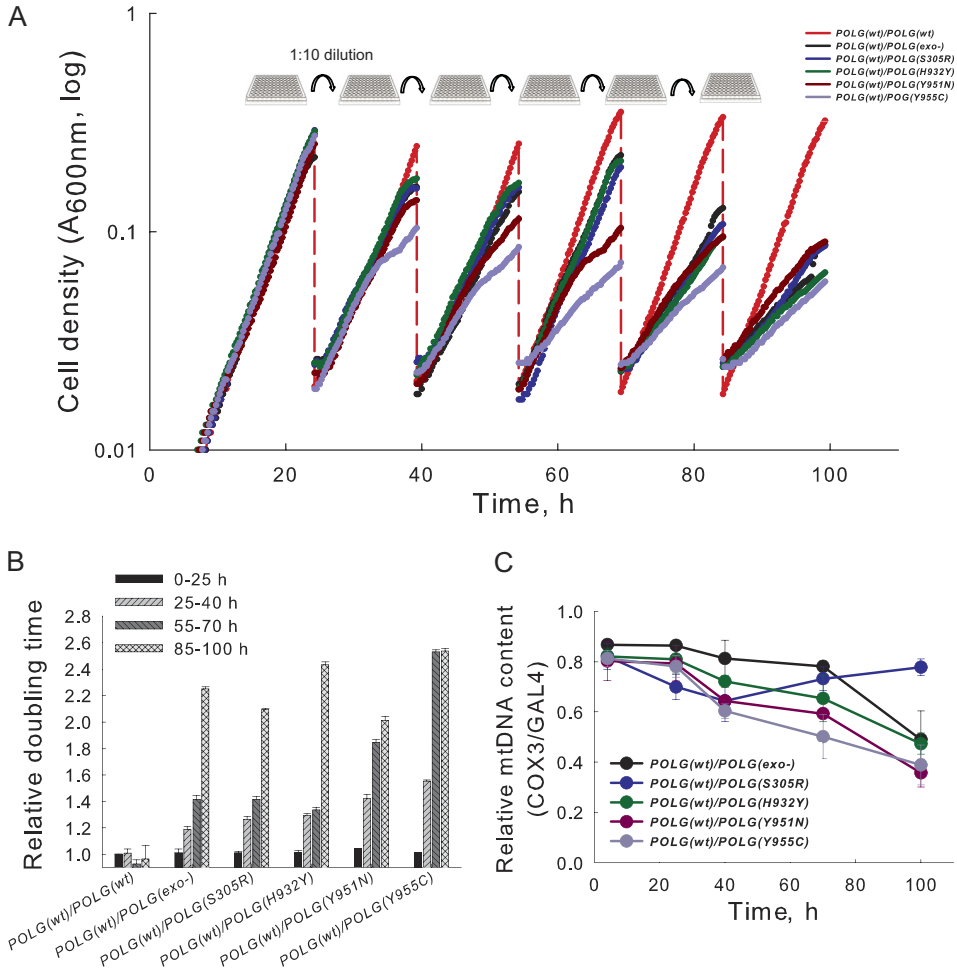

FIGURE 6. **Continuous growth phenotype of heterozygous diploid strains.** *A*, growth curve profiles of successive dilutions of heterozygous diploid strains in synthetic medium (−ura) supplemented with 2.5% glycerol. Growth conditions were maintained at 30 °C with continuous shaking. Cultures were inoculated to 10^5 cells/ml at the beginning and allowed to grow until an A_{600} of 0.2, when the first dilution (1:10) was made into fresh medium. The experiments were conducted for six successive cycles (~30 culture generations), and the doubling time of each cycle for each heterozygous diploid strain is summarized in *B*. *C*, relative mtDNA content of cells from the continuous growth culture. Genomic DNA was extracted from cells harvested at the end of each growth cycle. The *COX3/GAL4* ratio was normalized to 1 for *POLG(WT)/POLG(WT)* diploid cells. *Error bars*, S.D.

phase and has been proposed as a model of aging in postmitotic cells of higher organisms (45). We measured the viability of the aged yeast cells growing on glucose (Fig. 8*A*). As expected, the CLS values of mutant strains (*exo*$^-$, *H932Y*, and *Y955C*) were significantly shorter than that of wild-type Pol-γ *exo*$^+$ strain. For the *H932Y* heterozygous diploid strain, roughly 50% of cells died 3 days after entering stationary phase. Interestingly, the *mip1*/*POLG exo*$^+$ strain showed the same CLS as wild type, and S305R mutation caused only minor effects on CLS. To further explore the role of mitochondrial function on aging, we measured the mtDNA content of cells as a function of time in stationary phase. As shown in Fig. 8*B*, the significant age-dependent mtDNA content reduction was detected for all mutants. The measured mtDNA damage (mutation and depletion) is expected to in turn affect mitochondrial membrane function. We then calculated the relative $\Delta\psi m$ using the ratio of mean intensity of FL-1 over the mean intensity of FL-2 and plotted it against the aging time. As shown in Fig. 8*C*, the depolarization of mitochondria for mutants shared a similar trend with the viability assay (Fig. 8*A*), indicating that mutant heterozygous diploid cells showed a progressive decline in function manifesting in loss of $\Delta\psi m$, which appeared to precede the loss of mtDNA content.

Human Disease Onset Is Correlated with Time of Onset of Growth Defects in Yeast—Mitochondrial disorders stemming from mutations in the Pol-γ show widely varying severity of symptoms and differing delayed onset, leading to the postulate that mitochondrial disorders result from the accumulation of DNA damage (13). Here we have tested this theory using diploid strains of humanized yeast harboring mutations associated with heritable human diseases. We have sought to test whether the age of onset in humans is attributable more to reduced rates of polymerization or increased mutation frequency. Although accumulation of deletions may also play a role, we have not fully quantified those effects in this study.

As shown in Fig. 9*A*, for the mutants characterized here, the yeast mean survival time is negatively correlated with mutation frequency, measured from the rates of emergence of erythromycin resistance. There is no correlation between the reduced k_{cat}/K_m values measured for purified enzymes harboring different mutations and the yeast mean survival

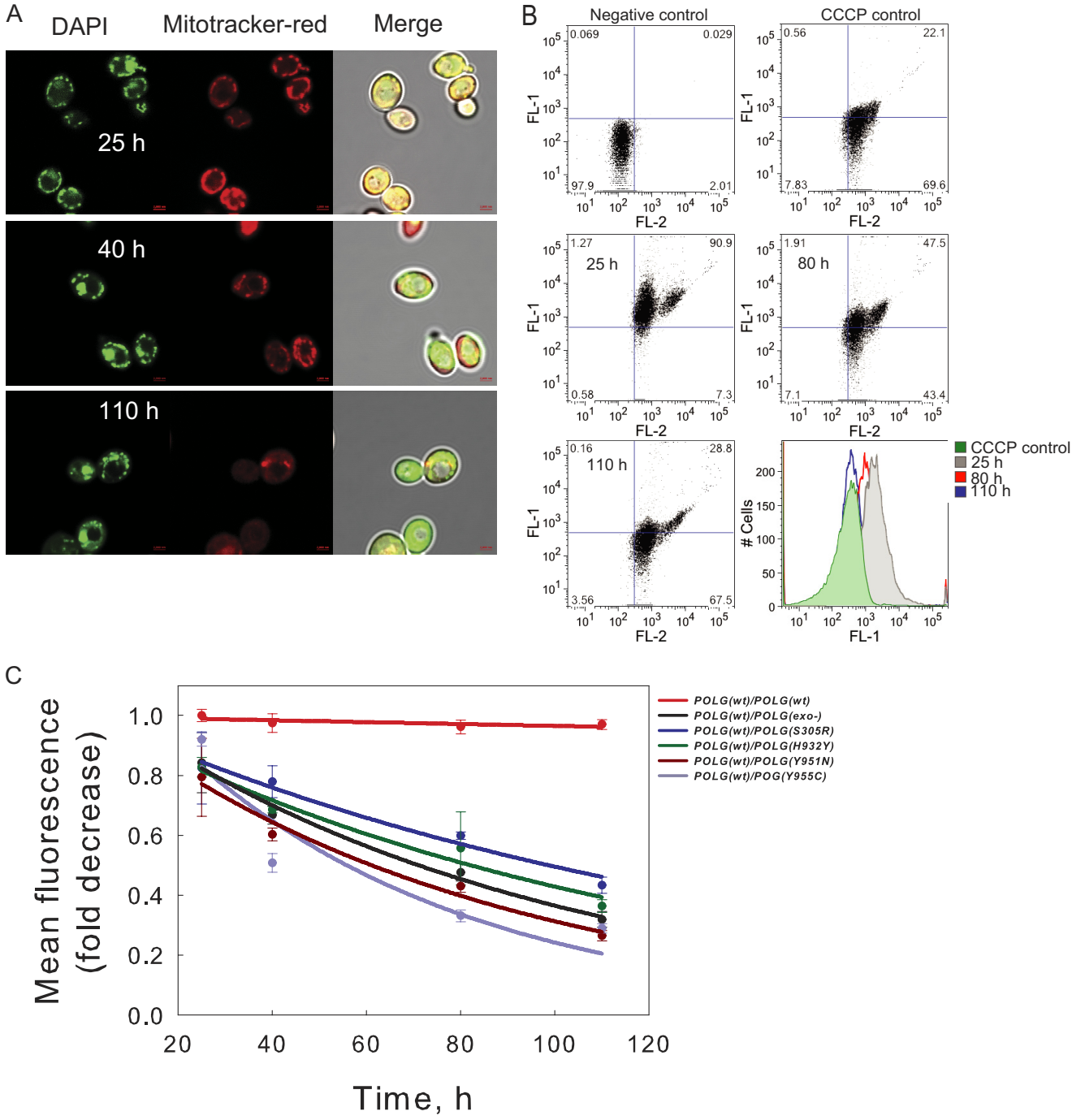

FIGURE 7. **Progressive growth deficiency is correlated with mitochondrial membrane depolarization.** *A*, representative confocal microscopy images of heterozygous diploid cells (*POLG(WT)/POLG(Y955C)*). The cells were harvested from the end of each cycle of continuous growth on glycerol and stained with MitoTracker Red (500 nM) and DAPI (1 ng/ml). *B*, flow cytometry analysis of mitochondrial membrane potential ($\Delta\psi m$) of heterozygous diploid cells (*POLG(WT)/POLG(Y955C)*) growing through successive dilutions. Cells grown from the end of each round of dilution were washed and resuspended in PBS and labeled with JC-1 (5 μM) and then analyzed by flow cytometry, as described under "Experimental Procedures." The negative control represents the fluorescence profile of cells without labeling. The carbonyl cyanide *m*-chlorophenyl hydrazone control represents the fluorescence profile of cells with depolarized membrane. *C*, time-dependent fluorescence change (*FL-1*) of heterozygous diploid cells stained with JC-1 from continuous growth culture. The data were fitted to a single-exponential decay to extract the decay rate. *Error bars*, S.D.

time or the age of disease onset observed in humans (Fig. 9, *B* and *C*). However, there is an apparent correlation between the onset of growth defects in yeast and the age of disease onset in humans (Fig. 9*D*) for those mutations with good evidence supporting a cause/effect relationship based upon human genetic studies.

DISCUSSION

In this paper, we sought to provide a link between the measurable biochemical defects caused by specific point mutations in Pol-γ with their associated physiological consequences and resulting phenotypes described clinically. Studies from our laboratory and others have quantified the effects of Pol-γ point

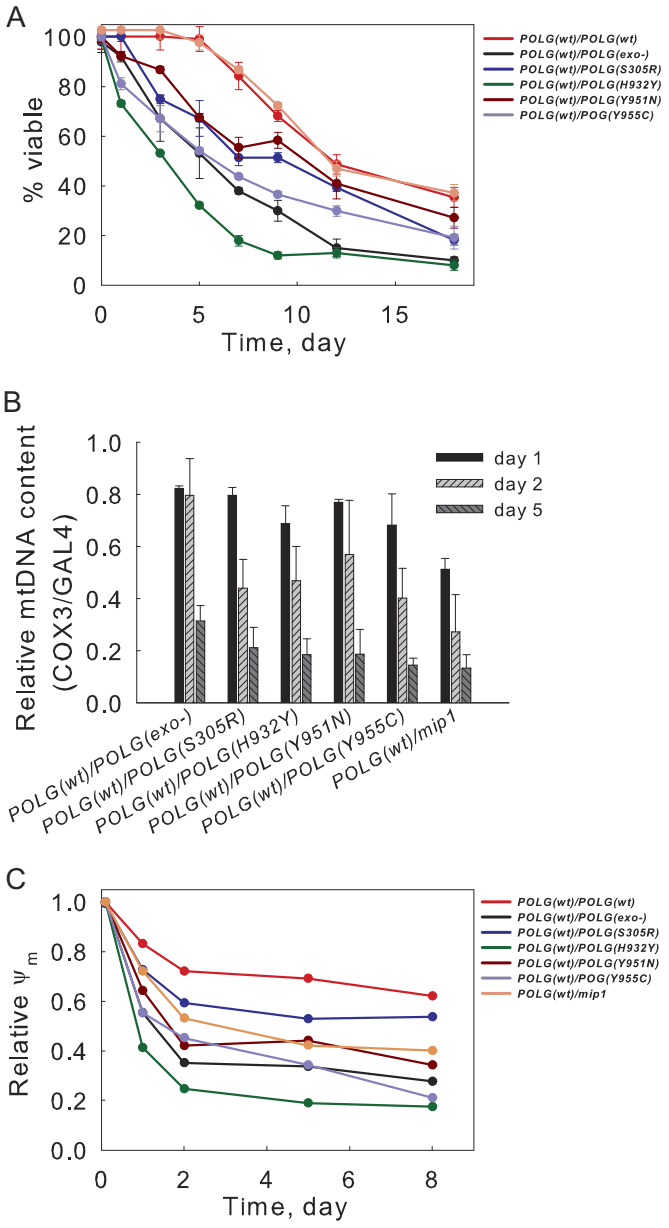

FIGURE 8. **Effect of mitochondrial function in chronological aging.** *A*, life span curves (percentage viability *versus* days in stationary phase) of heterozygous diploid strains over 2 weeks, determined by cfu counts on solid SD medium. *B*, age-dependent mtDNA content change of heterozygous diploid cells. *C*, loss of mitochondrial membrane potential ($\Delta\psi m$) during chronological aging. The relative $\Delta\psi m$ values (as described under "Experimental Procedures") were determined by flow cytometry of aged heterozygous diploid cells stained with JC-1. *Error bars*, S.D.

mutations on efficiency and fidelity of DNA replication *in vitro*, suggesting that accurate biochemical measurements can provide a basis to rationalize clinical observations (8–11). However, there are significant complexities in extrapolating from quantitative measurements of the effects of point mutations on DNA replication rate and fidelity *in vitro* to the final physiological consequences in humans. In particular, the interplay of wild-type and mutant alleles (recessive/dominant mutation) raises many questions that cannot be answered without studying the effects of mutations in the context of mitochondrial replication within living cells. Here we show indeed that the wild-type allele largely compensates for defects in the mutant forms of Pol-γ, especially those defects leading to slower rates of polymerization.

Using the humanized yeast as a model, we have provided a novel analysis to correlate the physiological consequences of point mutations in the human mitochondrial DNA polymerase with measurements of activity *in vitro*. Our results demonstrate that human Pol-γ can efficiently complement *mip1* deletion mutants in yeast and that complementation can be improved by the addition of the Pol-γB accessory protein. The slight growth deficiency of humanized yeast as compared with the wild type (Fig. 2*B*) may be in part due to the decrease in the polymerization rate of human Pol-γ at 30 °C compared with 37 °C. Nonetheless, humanized yeast haploid cells showed a growth rate and spontaneous mtDNA mutation rate comparable with that of MIP1 wild-type cells (Fig. 2*B* and Table 1), indicating that human Pol-γ can function together with the endogenous yeast mitochondrial DNA replicative components at the replication fork for accurate DNA synthesis.

Notably, the helicase involved in mtDNA replication in yeast has yet to be identified, and the yeast genome does not encode a homologue of the human mitochondrial DNA helicase. Although two DNA helicases (Pif1p and Hmip) are imported into yeast mitochondria, they are primarily linked with mtDNA recombination and maintenance rather than in DNA replication (46, 47). Thus, future study is needed to identify the endogenous helicase that functions with human Pol-γ during mtDNA replication in humanized yeast. Despite differences in mtDNA structure and replication models between human and yeast, common fundamental mechanisms of replication are retained sufficiently to support replication. Our data provide tangible support for the functional conservation of enzymes required for mitochondrial DNA replication.

The complementation by Pol-γ enables us to study the effects of Pol-γ mutations. Three of the mutations chosen for study (H932Y, Y951N, and Y955C) affect the Pol-γA polymerase active site. The H932Y mutation reduces the specificity constant governing correct nucleotide incorporation 150-fold but does not significantly affect the maximal rate of polymerization (8). The Y955C mutant of Pol-γ showed an ~8-fold decrease in maximal rate of polymerization and a 155-fold increase in the K_m for correct incorporation, thus resulting in a ~1300-fold decrease in efficiency as measured by k_{cat}/K_m (9). Mutation Y951N in Pol-γ caused an 11-fold reduction in the rate of replication.[4] In accordance with the *in vitro* data, haploid cells harboring either the H932Y, Y951N, or Y955C mutation in Pol-γ were unable to respire using glycerol as the sole carbon source (Fig. 3*B*). The suspicion that these cells had lost their mitochondria was confirmed by the absence of DAPI and MitoTracker Red staining by confocal microscopy (Fig. 3*E*) and also by qPCR (Fig. 3*C*). We were unable to examine the mtDNA mutation frequency for these three mutations in haploid cells due to their inabilities to grow on glycerol. Nevertheless, *in vitro* measurements of H932Y and Y955C Pol-γ mutants show that they readily extended multiple mismatches to decrease the overall fidelity by suppressing the contribution of the proofreading exonuclease (8, 9). In heterozygous diploid cells, mtDNA mutation frequency (measured after ~5–6 genera-

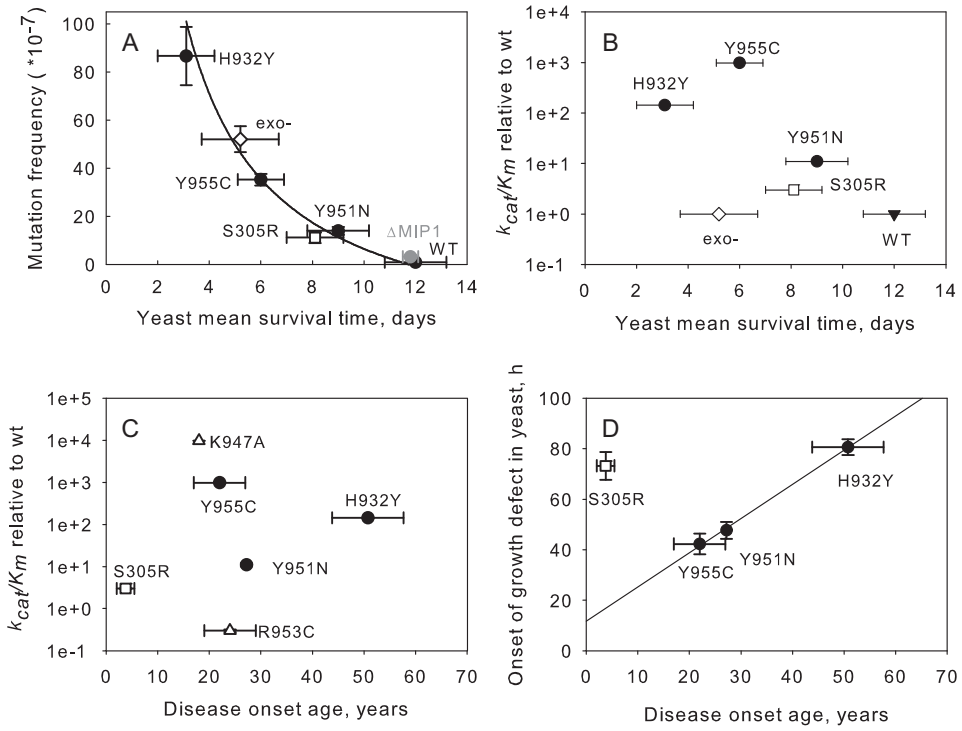

FIGURE 9. **The yeast onset of growth defect and aging can mimic the human disease onset.** *A*, correlation of the mtDNA mutation frequency with the median survival time of cells in the stationary phase. The -fold decrease of replication rates (k_{cat}/K_m) measured by single turnover nucleotide incorporation for Pol-γ mutants indicated refer to footnote 4 relative to the wild-type enzyme were plotted against the median survival time of cells in the stationary phase (*B*) and the onset ages of mitochondria disorders associated with the mutations in Pol-γ (*C*). *D*, the half-time of the growth defect onset of the heterozygous diploid cells (S305R, H932Y, Y951N, and Y955C) from the continuous growth was correlated with the disease onset ages. *Error bars*, S.D.

tions) increased to ~70-fold and ~20-fold for mutants carrying H932Y and Y955C mutation, respectively. Thus, decreased replication fidelity may be a major consequence of these point mutations.

To further demonstrate the significant role of enzyme fidelity in mtDNA maintenance, we studied mutations D198A/E200A and S305R, which are located in the exonuclease and linker domains of the polymerase, respectively. Exonuclease activity-deficient (D198A/E200A) haploid cells exhibited a ~70-fold increase in Ery^R frequencies (Table 1), although cells could grow poorly in glycerol (Fig. 3*B*). Continuous growth in glycerol over ~40 generations eventually results in 100% petite cells, due to the accumulation of mtDNA mutations and deletions, possibly compounded by the accelerated oxidative stress. The biochemical characterization of S305R mutation in Pol-γ revealed a 3–10-fold decrease in the proofreading exonuclease excision rate of mismatched base pairs and a ~3-fold reduction in the replication rate (Fig. 4). The S305R mutation in haploid yeast was quite detrimental, giving rise to nearly 100% petite cells and a complete loss of functional mitochondria (Table 1 and Fig. 3*E*).

Our data are consistent with studies in humans, which have shown that mtDNA mutations accumulate with aging in several tissues of humans (48, 49) and subsequently cause mtDNA deletion and respiration chain deficiency. The significant role of high mtDNA mutation rates in mitochondrial dysfunction is also supported by the mouse model carrying homozygous Pol-γ *exo*$^-$ mutations (50, 51), which resulted in a premature aging phenotype.

It is reasonable to postulate that both the replication rate and the enzyme fidelity may lead to the observed phenotype in haploid cells. Nevertheless, the role of the replication rate appears to be minor, due to the compensation by the wild-type enzyme in heterozygous diploid cells (Fig. 5), as reflected by the functional mitochondria and retention of over 50% of mtDNA content relative to wild type. Most strikingly, all mutant heterozygous diploid cells grown in glycerol showed a lag time and growth rate similar to the wild-type cells at the beginning of growth (Fig. 5*B*), in contrast to the much longer lag time of *mip1*/*POLG(WT)* cells. It has been reported that genes involved in mitochondrial function and protection from oxidative stress are significantly up-regulated for the entry into and exit from the stationary phase (52). The *mip1*/*POLG(WT)* cells contain ~50% mtDNA relative to the *POLG(WT)*/*POLG(WT)* cells (Fig. 5*C*) and thus may require a longer time to up-regulate POLG expression and to synthesize mtDNA to pass the transition. For heterozygous diploid mutant cells, both wild-type and mutant copy are likely to be actively involved in mtDNA replication. However, mtDNA mutations will accumulate over time and may reach a threshold sufficient to generate a dominant (negative) physiological effect (Fig. 5*B*).

Our working hypothesis is further supported by the continuous growth experiments performed by successive dilutions into fresh medium (Fig. 6*A*) to circumvent complex changes in metabolism as cells enter stationary phase. Cells harboring the Y951N mutation exhibited much earlier onset of growth defects than for the S305R mutation despite their similar replication rates at physiological nucleotide concentrations (Fig.

6*A*).[4] This again argues for the minor role of the replication rate, suggesting that the interplay between wild-type and mutant enzyme determines the overall observed rate and accuracy of mtDNA replication. In particular, the S305R mutant protein showed a ~20-fold decrease of the apparent DNA binding affinity compared with wild type. Therefore, the detrimental effects of the S305R mutant enzyme could be suppressed by the presence of wild-type protein *in vivo* due to its weaker DNA binding affinity. In contrast, Y951N mutant may compete with wild type on the replication origin site due to a comparable DNA binding affinity,[4] resulting in early onset of the growth defect. Similar dominant effects were also observed for Y955C mutants (Fig. 5, *A* and *B*) (9, 11).

Our analysis suggests that the primary effect leading to early onset of growth defects is likely to be the increased mutation frequency, not an decreased polymerization rate. In Fig. 9*A*, we show a direct correlation between mutation frequency and the yeast mean survival time. To approximate this dependence, we have fit the correlation curve to a hyperbolic function, but other functions may be more appropriate. The correlation is not expected to be linear, but it does predict a maximum survival time in the limit where the mutation frequency approaches zero, suggesting other physiological constraints on survival. At the opposite limit, one can reasonably expect that survival time will asymptotically approach zero as the mutation frequency increases. Most importantly, we observed a clear correlation of the onset of the phenotypes for heterozygous diploid cells with the disease onset age (Fig. 9*D*), which is independent of the enzyme's replication efficiency as defined by the k_{cat}/K_m value (Fig. 9*C*). Note that we have excluded S305R from the analysis in Fig. 9*D* because there is no clear link between the single point mutation and the heritable disease; rather, it appears that other mutations in *trans* contribute to the observed clinical phenotypes (13, 53). Our results imply that the single mutation S305R, heterozygous with wild-type *POLG*, is unlikely to be significantly detrimental because the wild-type allele sufficiently complements defects in replication. Thus, our methods can help to sort out the often complex human genetic analysis in looking for correlations between point mutations and human disease. Further work is planned to examine the effects of multiple mutations.

POLG mutations exhibit a broad clinical spectrum of mitochondrial disorders. There is no apparent correlation between observed yeast mtDNA content with the disease severity or the age of disease onset in humans (13). In accord with the clinical data, the mtDNA content reduction did not seem to completely correlate with the progressive growth deficiency in heterozygous diploid cells (Fig. 6, *A* and *C*), suggesting that other factors are also causing the mitochondrial damage (*i.e.* mutations and mtDNA deletion). Our data suggest that reductions in mtDNA content may lag behind the initial accumulation of mutations and deletions that are likely to be the primary cause of disease phenotypes. The mitochondrial membrane potential is another way of evaluating the mitochondrial function because it depends on an active electron transport chain. Accordingly, we observed that mitochondrial depolarization was clearly associated with the oxidative growth defects (Fig. 7*C*) in continuous growth experiments and preceded the observed reduction in mtDNA content. The mitochondrial depolarization may be due to mutations in ATP synthase as described in a previous study (54), although our results could not differentiate whether the mitochondrial depolarization is a marker of the progressive oxidative growth defects or the mitochondrial depolarization is causing the latter phenotype.

The mutations linked to PEO mostly affect the postmitotic tissues and are correlated with the mtDNA deletions and depletions (55, 56). Measurements of CLS in heterozygous diploid cells can provide information on the effects of these mutations in non-dividing cells. The heterozygous diploid cells harboring PEO-associated mutations (H932Y or Y955C) significantly curtailed CLS (Fig. 6*A*). Postmitotic cells have much lower levels of dNTP pools, and the negative effects of H932Y and Y955C mutation in mtDNA synthesis may begin to dominate due to the 150- or 160-fold increase in the K_d for correct nucleotide binding, respectively. The slower rate of nucleotide incorporation may cause polymerase stalling that can increase deletions or mutagenesis (Table 1), which could result in dysfunctional, depolarized mitochondria that would be targeted for degradation by autophagosomes (43).

As with many model systems, in this case, one must ponder how observations of cell growth in yeast over the period of a few days can be predictive of the progression of diseases in humans that develop over the course of years. In part, the faster onset of the phenotype in yeast could be attributable to growth on a single carbon source requiring oxidative metabolism, which could add additional oxidative stress and demands on mtDNA replication. Alternatively, there could be repair mechanisms or other adaptive responses in human tissues that extend the lag period leading to the onset of symptoms. In either case, our studies provide good evidence in support of the utility of the yeast system, and further studies using this system should afford a novel method to unravel the complex series of events from biochemical defect to physiological symptoms.

REFERENCES

1. Johnson, A. A., Tsai, Y. C., Graves, S. W., and Johnson, K. A. (2000) Human mitochondrial DNA polymerase holoenzyme. Reconstitution and characterization. *Biochemistry* **39,** 1702–1708
2. Johnson, A. A., and Johnson, K. A. (2001) Exonuclease proofreading by human mitochondrial DNA polymerase. *J. Biol. Chem.* **276,** 38097–38107
3. Spelbrink, J. N., Li, F. Y., Tiranti, V., Nikali, K., Yuan, Q. P., Tariq, M., Wanrooij, S., Garrido, N., Comi, G., Morandi, L., Santoro, L., Toscano, A., Fabrizi, G. M., Somer, H., Croxen, R., Beeson, D., Poulton, J., Suomalainen, A., Jacobs, H. T., Zeviani, M., and Larsson, C. (2001) Human mitochondrial DNA deletions associated with mutations in the gene encoding Twinkle, a phage T7 gene 4-like protein localized in mitochondria, *Nat. Genet.* **28,** 223–231
4. Qian, Y., Ziehr, J. L., and Johnson, K. A. (2013) Towards efficient reconstitution of the human mitochondrial DNA replication complex. *Biophys. J.* **104,** 74a
5. Korhonen, J. A., Pham, X. H., Pellegrini, M., and Falkenberg, M. (2004) Reconstitution of a minimal mtDNA replisome *in vitro*. *EMBO J.* **23,** 2423–2429
6. Stumpf, J. D., and Copeland, W. C. (2011) Mitochondrial DNA replication and disease. Insights from DNA polymerase γ mutations. *Cell. Mol. Life Sci.* **68,** 219–233
7. Copeland, W. C. (2008) Inherited mitochondrial diseases of DNA replication. *Annu. Rev. Med.* **59,** 131–146
8. Batabyal, D., McKenzie, J. L., and Johnson, K. A. (2010) Role of histidine 932 of the human mitochondrial DNA polymerase in nucleotide discrim-

ination and inherited disease. *J. Biol. Chem.* **285,** 34191–34201
9. Estep, P. A., and Johnson, K. A. (2011) Effect of the Y955C mutation on mitochondrial DNA polymerase nucleotide incorporation efficiency and fidelity. *Biochemistry* **50,** 6376–6386
10. Kasiviswanathan, R., and Copeland, W. C. (2011) Biochemical analysis of the G517V POLG variant reveals wild-type like activity. *Mitochondrion* **11,** 929–934
11. Atanassova, N., Fusté, J. M., Wanrooij, S., Macao, B., Goffart, S., Bäckström, S., Farge, G., Khvorostov, I., Larsson, N. G., Spelbrink, J. N., and Falkenberg, M. (2011) Sequence-specific stalling of DNA polymerase γ and the effects of mutations causing progressive ophthalmoplegia. *Hum. Mol. Genet.* **20,** 1212–1223
12. Graziewicz, M. A., Longley, M. J., Bienstock, R. J., Zeviani, M., and Copeland, W. C. (2004) Structure-function defects of human mitochondrial DNA polymerase in autosomal dominant progressive external ophthalmoplegia. *Nat. Struct. Mol. Biol.* **11,** 770–776
13. Tang, S., Wang, J., Lee, N. C., Milone, M., Halberg, M. C., Schmitt, E. S., Craigen, W. J., Zhang, W., and Wong, L. J. (2011) Mitochondrial DNA polymerase γ mutations. An ever expanding molecular and clinical spectrum. *J. Med. Genet.* **48,** 669–681
14. Lee, Y. S., Kennedy, W. D., and Yin, Y. W. (2009) Structural insight into processive human mitochondrial DNA synthesis and disease-related polymerase mutations. *Cell* **139,** 312–324
15. Di Fonzo, A., Bordoni, A., Crimi, M., Sara, G., Del Bo, R., Bresolin, N., and Comi, G. P. (2003) POLG mutations in sporadic mitochondrial disorders with multiple mtDNA deletions. *Hum. Mutat.* **22,** 498–499
16. Van Goethem, G., Dermaut, B., Lofgren, A., Martin, J. J., and Van Broeckhoven, C. (2001) Mutation of POLG is associated with progressive external opthalmoplegia characterized by mtDNA deletions. *Nat. Genet.* **28,** 2
17. Sohl, C. D., Kasiviswanathan, R., Copeland, W. C., and Anderson, K. S. (2013) Mutations in human DNA polymerase γ confer unique mechanisms of catalytic deficiency that mirror the disease severity in mitochondrial disorder patients. *Hum. Mol. Genet.* **22,** 1074–1085
18. Shadel, G. S. (1999) Yeast as a model for human mtDNA replication. *Am. J. Hum. Genet.* **65,** 1230–1237
19. Foury, F., and Kucej, M. (2002) Yeast mitochondrial biogenesis. A model system for humans? *Curr. Opin. Chem. Biol.* **6,** 106–111
20. Steinmetz, L. M., Scharfe, C., Deutschbauer, A. M., Mokranjac, D., Herman, Z. S., Jones, T., Chu, A. M., Giaever, G., Prokisch, H., Oefner, P. J., and Davis, R. W. (2002) Systematic screen for human disease genes in yeast. *Nat. Genet.* **31,** 400–404
21. Rinaldi, T., Dallabona, C., Ferrero, I., Frontali, L., and Bolotin-Fukuhara, M. (2010) Mitochondrial diseases and the role of the yeast models. *FEMS Yeast Res.* **10,** 1006–1022
22. Shutt, T. E., and Gray, M. W. (2006) Bacteriophage origins of mitochondrial replication and transcription proteins, *Trends Genet.* **22,** 90–95
23. Stuart, G. R., Santos, J. H., Strand, M. K., Van Houten, B., and Copeland, W. C. (2006) Mitochondrial and nuclear DNA defects in *Saccharomyces cerevisiae* with mutations in DNA polymerase γ associated with progressive external ophthalmoplegia. *Hum. Mol. Genet.* **15,** 363–374
24. Baruffini, E., Ferrero, I., and Foury, F. (2007) Mitochondrial DNA defects in *Saccharomyces cerevisiae* caused by functional interactions between DNA polymerase γ mutations associated with disease in human. *Biochim. Biophys. Acta* **1772,** 1225–1235
25. Stumpf, J. D., Bailey, C. M., Spell, D., Stillwagon, M., Anderson, K. S., and Copeland, W. C. (2010) mip1 containing mutations associated with mitochondrial disease causes mutagenesis and depletion of mtDNA in *Saccharomyces cerevisiae*. *Hum. Mol. Genet.* **19,** 2123–2133
26. Szczepanowska, K., and Foury, F. (2010) A cluster of pathogenic mutations in the 3′–5′ exonuclease domain of DNA polymerase γ defines a novel module coupling DNA synthesis and degradation. *Hum. Mol. Genet.* **19,** 3516–3529
27. Baruffini, E., Horvath, R., Dallabona, C., Czermin, B., Lamantea, E., Bindoff, L., Invernizzi, F., Ferrero, I., Zeviani, M., and Lodi, T. (2011) Predicting the contribution of novel POLG mutations to human disease through analysis in yeast model. *Mitochondrion* **11,** 182–190
28. Fontanesi, F., Palmieri, L., Scarcia, P., Lodi, T., Donnini, C., Limongelli, A., Tiranti, V., Zeviani, M., Ferrero, I., and Viola, A. M. (2004) Mutations in AAC2, equivalent to human adPEO-associated ANT1 mutations, lead to defective oxidative phosphorylation in *Saccharomyces cerevisiae* and affect mitochondrial DNA stability. *Hum. Mol. Genet.* **13,** 923–934
29. Viikov, K., Väljamäe, P., and Sedman, J. (2011) Yeast mitochondrial DNA polymerase is a highly processive single-subunit enzyme. *Mitochondrion* **11,** 119–126
30. Walter, M. C., Czermin, B., Muller-Ziermann, S., Bulst, S., Stewart, J. D., Hudson, G., Schneiderat, P., Abicht, A., Holinski-Feder, E., Lochmüller, H., Chinnery, P. F., Klopstock, T., and Horvath, R. (2010) Late-onset ptosis and myopathy in a patient with a heterozygous insertion in POLG2. *J. Neurol.* **257,** 1517–1523
31. Ferraris, S., Clark, S., Garelli, E., Davidzon, G., Moore, S. A., Kardon, R. H., Bienstock, R. J., Longley, M. J., Mancuso, M., Gutiérrez Ríos, P., Hirano, M., Copeland, W. C., and DiMauro, S. (2008) Progressive external ophthalmoplegia and vision and hearing loss in a patient with mutations in POLG2 and OPA1. *Arch. Neurol.* **65,** 125–131
32. Vogelsang, M., Comino, A., Zupanec, N., Hudler, P., and Komel, R. (2009) Assessing pathogenicity of MLH1 variants by co-expression of human MLH1 and PMS2 genes in yeast. *BMC Cancer* **9,** 382
33. Winderickx, J., Delay, C., De Vos, A., Klinger, H., Pellens, K., Vanhelmont, T., Van Leuven, F., and Zabrocki, P. (2008) Protein folding diseases and neurodegeneration. Lessons learned from yeast. *Biochim. Biophys. Acta.* **1783,** 1381–1395
34. Dunham, M. J., and Fowler, D. M. (2013) Contemporary, yeast-based approaches to understanding human genetic variation. *Curr. Opin. Genet. Dev.* **23,** 658–664
35. Franssens, V., Bynens, T., Van den Brande, J., Vandermeeren, K., Verduyckt, M., and Winderickx, J. (2013) The benefits of humanized yeast models to study Parkinson's disease. *Oxid. Med. Cell. Longev.* **2013,** 760629
36. Sherman, F. (1991) Getting started with yeast. *Methods Enzymol.* **194,** 3–21
37. Strathern, J. N., Klar, A. J., Hicks, J. B., Abraham, J. A., Ivy, J. M., Nasmyth, K. A., and McGill, C. (1982) Homothallic switching of yeast mating type cassettes is initiated by a double-stranded cut in the MAT locus. *Cell* **31,** 183–192
38. Storici, F., and Resnick, M. A. (2006) The delitto perfetto approach to *in vivo* site-directed mutagenesis and chromosome rearrangements with synthetic oligonucleotides in yeast. *Methods Enzymol.* **409,** 329–345
39. Merz, S., and Westermann, B. (2009) Genome-wide deletion mutant analysis reveals genes required for respiratory growth, mitochondrial genome maintenance, and mitochondrial protein synthesis in *Saccharomyces cerevisiae*. *Genome Biol.* **10,** R95
40. Fabrizio, P., and Longo, V. D. (2007) The chronological life span of *Saccharomyces cerevisiae*. *Methods Mol. Biol.* **371,** 89–95
41. Lee, Y. S., Lee, S., Demeler, B., Molineux, I. J., Johnson, K. A., and Yin, Y. W. (2010) Each monomer of the dimeric accessory protein for human mitochondrial DNA polymerase has a distinct role in conferring processivity. *J. Biol. Chem.* **285,** 1490–1499
42. Kalifa, L., and Sia, E. A. (2007) Analysis of Rev1p and Pol ζ in mitochondrial mutagenesis suggests an alternative pathway of damage tolerance. *DNA Repair* **6,** 1732–1739
43. Lee, J., Giordano, S., and Zhang, J. (2012) Autophagy, mitochondria and oxidative stress. Cross-talk and redox signalling. *Biochem. J.* **441,** 523–540
44. Smiley, S. T., Reers, M., Mottola-Hartshorn, C., Lin, M., Chen, A., Smith, T. W., Steele, G. D., Jr., and Chen, L. B. (1991) Intracellular heterogeneity in mitochondrial membrane potentials revealed by a J-aggregate-forming lipophilic cation JC-1. *Proc. Natl. Acad. Sci. U.S.A.* **88,** 3671–3675
45. Longo, V. D., Shadel, G. S., Kaeberlein, M., and Kennedy, B. (2012) Replicative and chronological aging in *Saccharomyces cerevisiae*. *Cell Metabolism* **16,** 18–31
46. Lahaye, A., Stahl, H., Thines-Sempoux, D., and Foury, F. (1991) Pif-1. A DNA helicase in yeast mitochondria. *EMBO J.* **10,** 997–1007
47. Kuusk, S., Sedman, T., Jõers, P., and Sedman, J. (2005) Hmi1p from *Saccharomyces cerevisiae* mitochondria is a structure-specific DNA helicase. *J. Biol. Chem.* **280,** 24322–24329
48. Bender, A., Krishnan, K. J., Morris, C. M., Taylor, G. A., Reeve, A. K., Perry, R. H., Jaros, E., Hersheson, J. S., Betts, J., Klopstock, T., Taylor, R. W., and Turnbull, D. M. (2006) High levels of mitochondrial DNA deletions in

substantia nigra neurons in aging and Parkinson disease. *Nat. Genet.* **38,** 515–517
49. Wang, Y., Michikawa, Y., Mallidis, C., Bai, Y., Woodhouse, L., Yarasheski, K. E., Miller, C. A., Askanas, V., Engel, W. K., Bhasin, S., and Attardi, G. (2001) Muscle-specific mutations accumulate with aging in critical human mtDNA control sites for replication. *Proc. Natl. Acad. Sci. U.S.A.* **98,** 4022–4027
50. Trifunovic, A., Wredenberg, A., Falkenberg, M., Spelbrink, J. N., Rovio, A. T., Bruder, C. E., Bohlooly-Y, M., Gidlöf, S., Oldfors, A., Wibom, R., Törnell, J., Jacobs, H. T., and Larsson, N. G. (2004) Premature ageing in mice expressing defective mitochondrial DNA polymerase. *Nature* **429,** 417–423
51. Kujoth, G. C., Hiona, A., Pugh, T. D., Someya, S., Panzer, K., Wohlgemuth, S. E., Hofer, T., Seo, A. Y., Sullivan, R., Jobling, W. A., Morrow, J. D., Van Remmen, H., Sedivy, J. M., Yamasoba, T., Tanokura, M., Weindruch, R., Leeuwenburgh, C., and Prolla, T. A. (2005) Mitochondrial DNA mutations, oxidative stress, and apoptosis in mammalian aging. *Science* **309,** 481–484
52. Martinez, M. J., Roy, S., Archuletta, A. B., Wentzell, P. D., Santa Anna-Arriola, S. S., Rodriguez, A. L., Aragon, A. D., Quiñones, G. A., Allen, C., and Werner-Washburne, M. (2004) Genomic analysis of stationary-phase and exit in *Saccharomyces cerevisiae*. Gene expression and identification of novel essential genes. *Mol. Biol. Cell* **15,** 5295–5305
53. Kurt, B., Jaeken, J., Van Hove, J., Lagae, L., Löfgren, A., Everman, D. B., Jayakar, P., Naini, A., Wierenga, K. J., Van Goethem, G., Copeland, W. C., and DiMauro, S. (2010) A novel POLG gene mutation in 4 children with Alpers-like hepatocerebral syndromes. *Arch. Neurol.* **67,** 239–244
54. Lai, C. Y., Jaruga, E., Borghouts, C., and Jazwinski, S. M. (2002) A mutation in the ATP2 gene abrogates the age asymmetry between mother and daughter cells of the yeast *Saccharomyces cerevisiae*. *Genetics* **162,** 73–87
55. Wanrooij, S., Luoma, P., van Goethem, G., van Broeckhoven, C., Suomalainen, A., and Spelbrink, J. N. (2004) Twinkle and POLG defects enhance age-dependent accumulation of mutations in the control region of mtDNA. *Nucleic Acids Res.* **32,** 3053–3064
56. Kollberg, G., Jansson, M., Pérez-Bercoff, A., Melberg, A., Lindberg, C., Holme, E., Moslemi, A. R., and Oldfors, A. (2005) Low frequency of mtDNA point mutations in patients with PEO associated with POLG1 mutations. *Eur. J. Hum. Genet.* **13,** 463–469